Structure of a NifS Homologue: X-ray Structure Analysis of CsdB, an *Escherichia coli* Counterpart of Mammalian Selenocysteine Lyase[†,‡]

Tomomi Fujii, Masaki Maeda, Hisaaki Mihara, Tatsuo Kurihara, Nobuyoshi Esaki,* and Yasuo Hata*[,§]

Institute for Chemical Research, Kyoto University, Uji, Kyoto 611-0011, Japan

Received July 27, 1999; Revised Manuscript Received October 29, 1999

ABSTRACT: *Escherichia coli* CsdB, a NifS homologue with a high specificity for L-selenocysteine, is a pyridoxal 5′-phosphate (PLP)-dependent dimeric enzyme that belongs to aminotransferases class V in fold-type I of PLP enzymes and catalyzes the decomposition of L-selenocysteine into selenium and L-alanine. The crystal structure of the enzyme has been determined by the X-ray crystallographic method of multiple isomorphous replacement and refined to an *R*-factor of 18.7% at 2.8 Å resolution. The subunit structure consists of three parts: a large domain of an α/β-fold containing a seven-stranded β-sheet flanked by seven helices, a small domain containing a four-stranded antiparallel β-sheet flanked by three α-helices, and an N-terminal segment containing two α-helices. The overall fold of the subunit is similar to those of the enzymes belonging to the fold-type I family represented by aspartate aminotransferase. However, CsdB has several structural features that are not observed in other families of the enzymes. A remarkable feature is that an α-helix in the lobe extending from the small domain to the large domain in one subunit of the dimer interacts with a β-hairpin loop protruding from the large domain of the other subunit. The extended lobe and the protruded β-hairpin loop form one side of a limb of each active site in the enzyme. The most striking structural feature of CsdB lies in the location of a putative catalytic residue; the side chain of Cys364 on the extended lobe of one subunit is close enough to interact with the γ-atom of a modeled substrate in the active site of the subunit. Moreover, His55 from the other subunit is positioned so that it interacts with the γ- or β-atom of the substrate and may be involved in the catalytic reaction. This is the first report on three-dimensional structures of NifS homologues.

Selenocysteine lyase (SCL,[1] EC 4.4.1.16) was characterized as the first enzyme specifically acting on the selenium-containing substrate (*1*, *2*). It is a pyridoxal 5′-phosphate (PLP)-dependent enzyme that catalyzes the removal of the selenium atom from L-selenocysteine to produce L-alanine but does not act on L-cysteine. Recently, it has been proposed that SCL facilitates selenophosphate synthesis (*3*). Selenium is specifically metabolized by such enzymes as selenophosphate synthetase (*4*), selenocysteine synthase (*5*), and selenocysteine methyltransferase (*6*). Specific recognition of selenium by these enzymes is important for the element to play a role as an essential trace element in mammals and other organisms (*7*). However, it remains unknown how these enzymes discriminate between two congeneric elements of sulfur and selenium.

Mouse cDNA encoding SCL has been cloned and sequenced, and its deduced amino acid sequence has been shown to be similar to those of NifS proteins (cysteine desulfurases) (H. Mihara, T. Kurihara, T. Watanabe, T. Yoshimura, and N. Esaki, unpublished results). NifS is a PLP-dependent enzyme that catalyzes the removal of the sulfur atom from L-cysteine to produce L-alanine. Thus, SCL and NifS catalyze the same type of reaction, the removal of a substituent at the β-carbon of L-selenocysteine or L-cysteine. SCL exclusively decomposes L-selenocysteine, while NifS acts not only on L-cysteine but also on L-selenocysteine. A reaction mechanism of NifS was proposed by Zheng et al. (*8*). In their proposal, the cysteinyl thiolate anion in the active site performs a nucleophilic attack on the sulfur of a substrate−PLP adduct, resulting in the formation of a cysteinyl persulfide and an enamine derivative of alanine. The NifS protein of *Azotobacter vinelandii* functions in nitrogen fixation by supplying sulfur to stabilize or repair the iron−sulfur cluster of the nitrogenase component protein (*9*). NifS homologues have been found in many nondiazotrophic procaryotes (*10*−*12*) and eucaryotes (*13*−*16*). These NifS homologues are proposed to play a general role in the mobilization of sulfur for iron−sulfur cluster

[†] This research was supported in part by Grants-in-aid for Scientific Research (10760048 to T.F., 11480179 to N.E., and 11169220 to Y.H.) from the Ministry of Education, Science, Sports, and Culture of Japan, a grant on Research for the Future from the Japan Society for the Promotion of Science (to N.E.), a research fellowship from the Japan Society for the Promotion of Science for Young Scientists (to H.M.), and the Sakabe project of TARA (Tsukuba Advanced Research Alliance) Center, University of Tsukuba, Y.H. being a TARA guest researcher.

[‡] The coordinates have been deposited in the Research Collaboratory for Structural Bioinformatics Protein Data Bank (file name 1C0N).

* To whom correspondence should be addressed. N.E.: telephone, +81-774-38-3240; fax, +81-774-38-3248; e-mail, esaki@scl.kyoto-u.ac.jp. Y.H.: telephone, +81-774-38-3251; fax, +81-774-38-3014; e-mail, hata@scl.kyoto-u.ac.jp.

[1] Abbreviations: CSD, cysteine sulfinate desulfinase; CsdB, *csdB* gene product; PLP, pyridoxal 5′-phosphate; NifS, *nifS* gene product; IscS, *iscS* gene product; SCL, selenocysteine lyase; AAT, aspartate aminotransferase; PSAT, phosphoserine aminotransferase; CBL, cystathionine β-lyase; PMA, phenylmercury acetate; MIR, multiple isomorphous replacement; SIR, single isomorphous replacement. Amino acid residues and secondary structural elements with numbers with an asterisk appended denote those belonging to the other subunit in the dimer molecule.

10.1021/bi991732a CCC: $19.00
Published on Web 01/21/2000

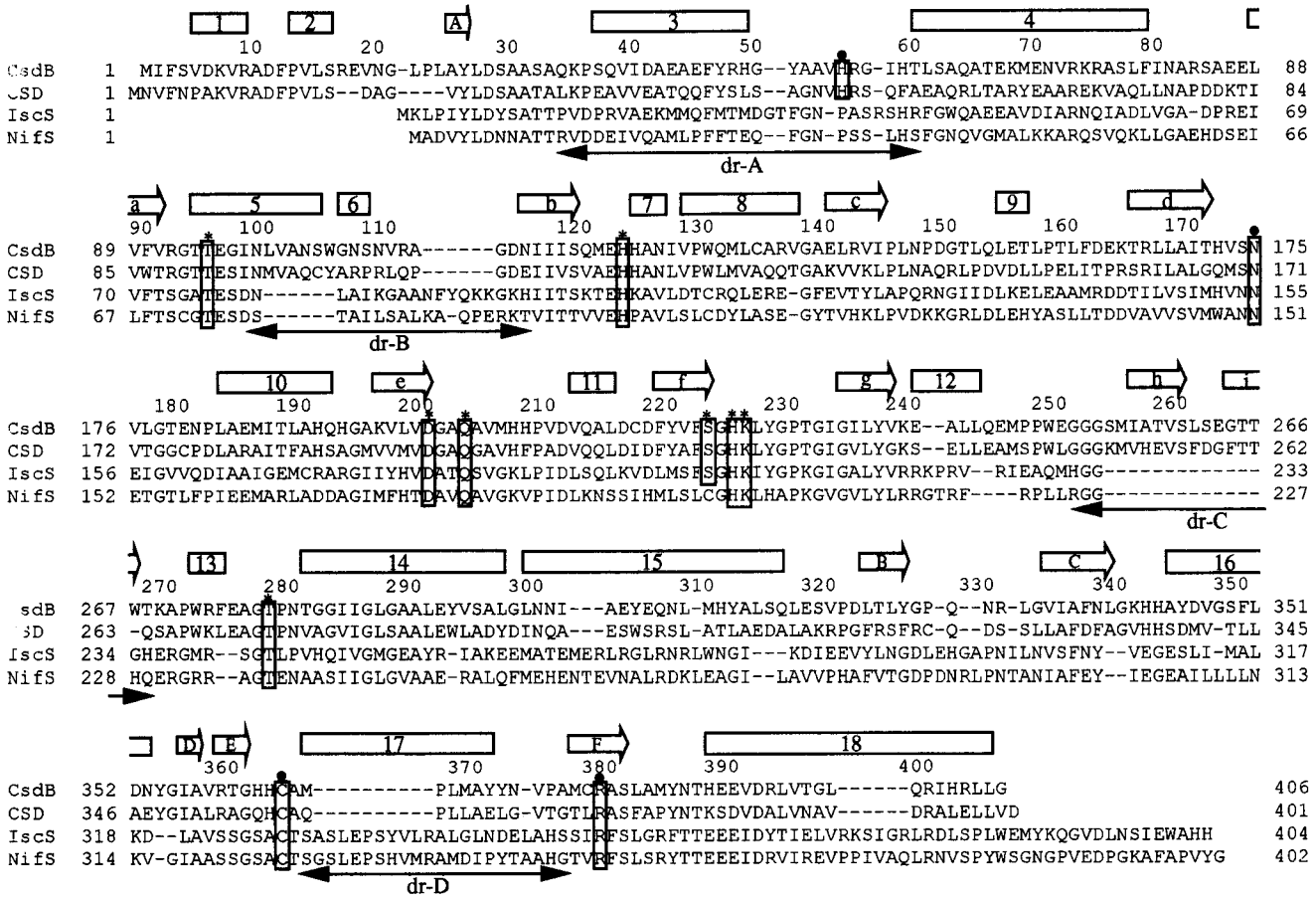

FIGURE 1: Sequence alignment of several NifS family proteins. Abbreviations: CsdB, product enzyme of the *csdB* gene from *E. coli*; CSD, cysteine sulfinate desulfinase from *E. coli*; IscS, product enzyme of the *iscS* gene from *E. coli*; NifS, product enzyme of the *nifS* gene in *A. vinelandii*. The numbering of the sequences is based on that of CsdB. The secondary structure elements of CsdB are denoted by rectangles with numbers for α- and 3_{10}-helices and arrows with letters for β-strands. The amino acid residues in boxes capped with * or ● interact with PLP or possibly with the substrate, respectively. The lines with arrows denote the regions (dr-A, dr-B, dr-C, and dr-D) whose sequences are different between groups I and II.

synthesis (*17*). However, it is also possible that some of these NifS homologues physiologically act as SCL that is specific for L-selenocysteine.

The *Escherichia coli* genome contains three genes which are homologous in nucleotide sequence to *nifS*: the *iscS* gene mapped at 57.3 min for the IscS protein, the *csdA* gene mapped at 63.4 min for cysteine sulfinate desulfinase (CSD), and the *csdB* gene mapped at 37.9 min for the CsdB protein. The amino acid sequence of CsdB is partially identical with those of CSD (44%), IscS (25%), and NifS from *A. vinelandii* (23%) (Figure 1). IscS and CSD are not specific toward L-selenocysteine. In contrast to these two enzymes, CsdB has high specific activity for L-selenocysteine relative to L-cysteine; the specific activity of CsdB toward L-selenocysteine is about 300 times higher than that toward L-cysteine (*18*). Thus, CsdB is regarded as an *E. coli* counterpart of the mammalian SCL.

CsdB forms a homodimer, and the subunit consists of 406 amino acid residues (M_r = 44 439) with one PLP molecule as a cofactor (*18*). PLP-dependent enzymes have been classified into seven distinct fold types on the basis of their similarity in primary structure, predicted secondary structure, and biochemical function (*19*). NifS proteins have been grouped as "aminotransferases class V" in fold-type I, together with aspartate β-decarboxylase (EC 4.1.1.12) (*20*) and kynureninase (EC 3.7.1.3) (*21*), which catalyze the removal of the β-substituent from the substrate to form alanine as NifS, serine-pyruvate aminotransferase, phosphoserine aminotransferase (PSAT), isopenicillin N epimerase, and the small subunit of cyanobacterial soluble hydrogenase. There has been no report on three-dimensional structures of this group of enzymes except for PSATs from *E. coli* and *Bacillus circulans* ssp. *alkalophilus* (*22*). Therefore, a structural analysis of CsdB will contribute to the understanding of the mechanism of the removal of the β-substituent from the substrate to form alanine and the catalytic mechanisms of other PLP-dependent enzymes. It will also provide useful information about the mechanism of enzymatic discrimination between selenium and sulfur in analogous substrates. Here, we report the crystal structure of CsdB at 2.8 Å resolution and discuss the relationships between the active site structure and the reaction mechanism. This is the first report on three-dimensional structures of NifS homologues.

MATERIALS AND METHODS

Crystallization and Heavy-Atom Screening. The overexpression, purification, and crystallization of CsdB were performed as described previously (*18*). Tetragonal-bipyramidal crystals were grown by a hanging-drop vapor-diffusion method of a 20 mg/mL enzyme solution against a 100 mM potassium phosphate buffer (pH 6.8) containing 1.4 M

sodium acetate and 10 μM PLP at 25 °C. A typical size for the crystals was approximately 0.5 mm × 0.5 mm × 0.4 mm. They belong to tetragonal space group $P4_32_12$, with the following unit cell dimensions: $a = b = 128.1$ Å and $c = 137.0$ Å. It was initially assumed that there were two subunits in the crystallographic asymmetric unit, and the crystal volume per unit mass, V_m, and the solvent content were estimated to be 3.19 Å^3/Da and 62%, respectively. These values fell within the ranges observed for general protein crystals (*23*). However, the self-rotation function calculated for native data with the program POLARRFN (*24*) was featureless. Moreover, the electron density map calculated with experimentally determined phases showed only one lump of the CsdB subunit in the asymmetric unit, as described later. These results revealed that the crystal of CsdB has one subunit in an asymmetric unit. Therefore, the present crystal of CsdB has an unusually high V_m value of 6.32 Å^3/Da, which corresponds to a high solvent content of 81%. The crystals diffract up to at least 2.8 Å resolution.

To solve the phase problem by the isomorphous replacement method, soaking conditions for preparing heavy-atom derivative crystals were searched by changing the kind and concentration of heavy-atom reagent and the soaking time. Two kinds of isomorphous heavy-atom derivative crystals were prepared by soaking the native crystals in the mother liquors containing 0.1 mM phenyl mercury acetate (PMA) for 24 h, and 30 mM $K_2Pt(CN)_4$ for 48 h, respectively.

Data Collection and Processing. Diffraction data for the native and two derivative crystals were collected at 20 °C on a Rigaku R-AXIS IIc imaging-plate detector system using Yale-type double-focusing-mirror monochromatized X-ray radiation produced by a Rigaku RU-300 rotating anode X-ray generator operated at 40 kV and 100 mA. The crystals were mounted with the crystallographic c^* axis parallel to the crystal rotation axis to record Bijvoet-mates for the heavy-atom derivatives on the same frame. The crystal-to-detector distance was set to 130 mm. Each of the 1.5° oscillation patterns was recorded for 10 min. A total of 33 frames for each data set covered diffraction spots within a rotation range of 50°. Data processing was accomplished up to 2.8 Å resolution for the native and two derivative crystals with the R-AXIS IIc data-processing software package. Diffraction data for each crystal were merged and scaled into a set of unique reflection data. The statistics of data collection and processing are summarized in Table 1.

Structure Determination and Refinement. The structure was determined by the multiple isomorphous replacement (MIR) method supplemented with anomalous scattering effects from the mercury derivative crystal. The determination of heavy-atom positions and the calculation of MIR phases were carried out using the programs PHASES (*25*) and MLPHARE in the CCP4 program suit (*24*), respectively. The difference Patterson map for each derivative was calculated at 5 Å resolution. One major site for mercury binding was found clearly on the Harker sections, and the other site was determined from an SIR difference Fourier map. The platinum-binding sites were obtained from an SIR cross-difference Fourier map and an MIR difference Fourier map. The mercury- and platinum-derivative crystals contained two and four binding sites per asymmetric unit, respectively. MIR phases were calculated up to 3.0 Å resolution, and relevant phase calculation statistics are summarized in Table 1. The overall figure of merit was 0.265. The MIR map was significantly improved by the iterative procedures of density modification and phase extension to 2.8 Å gradually performed with the program SOLOMON (*26*). Considering the crystallographic parameters of the present crystal and the molecular weight of the enzyme, the solvent content of the crystal initially seemed to be 62%, as described above. In the procedures of density modification, therefore, the solvent mask was applied as the solvent content of 60%. However, the improved electron density map did not show any significant density other than that for one subunit of the dimer molecule in the asymmetric unit. This result corresponds to the solvent content of 81% and indicates that the molecular 2-fold axis of the dimer coincides with the crystallographic 2-fold axis. Although the underestimated solvent content was used throughout the density modification, the resulting electron density map had a good quality that enabled us to trace not only the main chain but also most of the side chains. Thus, any recalculation with the higher solvent content was not required for the structural model building.

Table 1: Data Collection and Phase Calculation Statistics

	native	PMA	$K_2Pt(CN)_4$
data collection			
resolution limit (Å)	∞−2.8	∞−2.8	∞−2.8
no. of observed reflections ($I > 1\sigma_I$)	73138	58403	69180
no. of independent reflections ($I > 1\sigma_I$)	23770	20858	22914
completeness (%) (last shell[a])	94.2 (88.5)	90.1 (83.1)	91.5 (84.6)
R_{merge}[b] (%)	7.22	8.22	7.04
MIR analysis (3.0 Å)			
no. of sites		2	4
R_{iso}[c]		0.160	0.112
R_{Cullis}[d] (acentric/centric)		0.93/0.83	0.92/0.81
phasing power[e] (acentric/centric)		0.76/0.52	0.82/0.57
mean FOM[f] (MIR+AS[g])	0.265		

[a] The resolution limit for last shell is 3.0−2.8 Å. [b] $R_{merge} = \Sigma_i|I_i - \langle I_i\rangle|/\Sigma_i I_i$, where $\langle I_i\rangle$ is the average of I_i over all symmetry equivalents. [c] $R_{iso} = \Sigma||F_{PH}| - |F_P||/\Sigma|F_P|$, where F_{PH} and F_P are the derivative and native structure factors, respectively. [d] $R_{Cullis} = \Sigma||F_{PH}| \pm |F_P| - |F_H||/\Sigma||F_{PH}| \pm |F_P||$ for all centric reflections, where F_{PH} and F_P are the observed derivative and native structure factors, respectively, and F_H is the calculated heavy-atom structure factor. [e] Phasing power $= \langle F_H\rangle/\langle E\rangle$, where $\langle F_H\rangle$ is the rms calculated heavy-atom structure factor amplitude and $\langle E\rangle$ is the rms lack of closure error. [f] FOM is the figure of merit. [g] MIR+AS is the multiple isomorphous replacement method supplemented with anomalous scattering effects.

In the 2.8 Å resolution electron density map improved as described above, the phosphorus atom of PLP was identified above the 5σ level and was helpful in determining the location of PLP. Electron densities were skeletonized with the program xdlMAPMAN (*27*). The polypeptide chain was traced on the skeletonized map with the program O (*28*). The side chains of the polypeptide were assigned by reference to the primary structure deduced from the nucleotide sequence. The structural model was refined using a simulated annealing protocol of the program X-PLOR (*29*). A randomly selected 5% of all diffraction data were picked up and used for calculating the free *R*-factor from the beginning of the refinement. Individual atomic temperature factors as well as atomic positions were refined in further refinement cycles. During the course of refinement, the model was carefully

Table 2: Refinement Statistics

resolution limit (Å) (last shell)	8.0−2.8 (2.92−2.8)
no. of reflections ($F > 1\sigma_F$) (last shell)	21339 (2000)
R-factor (%)[a] (last shell)	18.7 (29.0)
R_{free} (%)[b] (last shell)	23.9 (34.5)
no. of atoms	
protein/PLP/acetate	3083/15/4
mean *B*-factors (Å^2)	
main chain/side chain/PLP/acetate	32.1/36.5/11.7/35.4
rms deviations from the ideal geometry	
bond lengths (Å)	0.003
bond angles (deg)	0.821
no. of residues in Ramachandran plot (%)[c]	
most favored/additional/disallowed	85.5/14.5/0.0

[a] *R*-factor = $100\Sigma||F_o| - |F_c||/\Sigma|F_o|$, where F_o and F_c are the observed and calculated structure factors, respectively. [b] R_{free} = *R*-factor which is calculated for a selected subset of the reflections (5%) excluded from the refinement. [c] Most favored, additional allowed, and disallowed regions are defined by PROCHECK.

inspected with $2F_o - F_c$ and $F_o - F_c$ maps and manually rebuilt in unreasonable regions using the program TurboFRODO (*30*). The accuracy of the model was assessed by calculating omit maps. The electron density flow for the region of His55−Ile58 was relatively ambiguous; in particular, Arg56 and Ile58 were modeled as alanine. The side chains of Lys7, Glu63, Lys164, and Lys341 could not be modeled beyond Cβ because of a lack of interpretable density. Four hundred and four residues (Phe3−Gly406), except two N-terminal disordered residues (Met1 and Ile2), and one PLP molecule were assigned in the electron density map.

There were several lumps of extra densities observed in the electron density map. The most conspicuous one was the extra density elongated beyond the Sγ atom of Cys364. The −SH group of Cys364 appeared to be modified by insertion of a single atom. Since it was difficult to identify the species of the inserted atom at the time, the modification of Cys364 was not made in the model presented here; this density feature is to be discussed later. A density peak other than those for the enzyme was observed among PLP and the side chains of Arg379 and Asn175. The peak was interpreted as an acetate (the precipitant for crystallization), because the ellipsoidal peak was surrounded by positively charged substituents. No water molecules giving significantly high electron density were found in the analysis presented here, although an acetate ion was found in the active site.

Finally, the refinement of the current model was converged to an *R*-factor of 18.7% for 21 339 reflections within the resolution range of 8.0−2.8 Å. The free *R*-factor was 23.9% for a randomly selected 5% of the data within the same resolution range (1090 reflections) (*31*). Refinement statistics are summarized in Table 2, and a typical electron density map around PLP in the refined structure is shown in Figure 2.

RESULTS

Overall Structure. The crystal structures of the CsdB subunit and the dimer molecule are represented in Figures 3 and 4, respectively. The CsdB crystal contains four homodimer molecules in the unit cell. The dimer molecules are positioned around the crystallographic 2-fold axes passing through (x, y, z) = (0, 0, 0), (0, 0, $^1/_2$), ($^1/_2$, $^1/_2$, $^1/_4$), and ($^1/_2$, $^1/_2$, $^3/_4$), and one subunit of each dimer is related to the other by the molecular 2-fold axis coinciding with one of the four crystallographic symmetry axes. The dimensions of the dimer are approximately 80 Å × 55 Å × 40 Å, and those of the subunit are approximately 60 Å × 55 Å × 35 Å. The present structural model of the CsdB subunit is composed of a polypeptide chain of Phe3−Gly406, one PLP, and one acetate. The crystal structure has good geometry. The rms deviations from ideal bond lengths and bond angles are 0.003 Å and 0.821°, respectively. The polypeptide dihedral angles (ϕ and ψ) for most non-glycine residues (85.5%) fall in the most favored regions defined by the program PROCHECK (*32*), with the remaining 14.5% in the additional allowed region and none in generally allowed or disallowed regions. The average temperature factors over the main chain atoms and the side chain atoms are 32.1 and 36.5 Å^2, respectively.

The secondary structural elements were identified with the program PROCHECK (*32*). They are denoted by numerals for helices and letters for β-strands in Figures 3B and 5. The topology diagram is depicted in Figure 5. The subunit folds into three spatially distinct parts: an N-terminal segment (residues 1−21), a central large PLP-binding domain (residues 33−298), and a small domain on the C-terminal side (residues 22−32 and 299−406). The N-terminal segment consists of helices 1 and 2 and makes contact with the large and small domains through several hydrophobic and some hydrophilic interactions. The segment is connected with the large domain through the long loop of residues 22−32 containing short β-strand A belonging to the small domain. The large domain has an α/β-fold structure comprising a seven-stranded mixed β-sheet (a, g, f, e, d, b, and c) flanked by seven α-helices (5−11), five additional α-helices (3, 4, and 12−14), and a small two-stranded antiparallel β-sheet (h and i). In the central β-sheet, the antiparallel β-sheet part (a, g, and f) and the parallel β-sheet part (f, e, d, b, and c) are mixed together with strand g antiparallel to the others, and each of the strands in the parallel β-sheet part is connected to the adjacent ones by α- or 3_{10}-helices crossing the β-sheet in a right-handed manner. Helices 9−11 are located on one side of the β-sheet to face the solvent area, and helices 5−8 lie in the interdomain interface on the opposite side. Short helices 7, 9, and 13 exhibit hydrogen-bonding patterns typical for 3_{10}-helices. PLP is covalently attached to the side chain of Lys226 to make a Schiff base and settled near the N-terminus of helix 5 and the C-termini of strands e and f. The most remarkable structural feature in the large domain lies in the protrusion of the β-hairpin loop containing the two-stranded antiparallel β-sheet (h and i). The loop plays a role in the formation of the dimer molecule and the intersubunit active site. The large domain and the small domain are connected together mainly by two helices (14 and 15). The small domain contains an α/β-structure, consisting of the four-stranded antiparallel β-sheet (B, C, F, and E) and three α-helices, and the small parallel β-bridge (A and D). The three helices (15, 16, and 18) are located on the solvent accessible side of the sheet. The most remarkable feature in the small domain lies in the extended lobe (residues 362−375) containing Cys364 and α-helix 17. The lobe extends from the small to the large domains of the subunit and plays an important role in forming the intersubunit active site by constituting one side of the entrance rim to the active site.

Two subunits tightly associate together to form a dimer, as shown in Figure 4. The interface for interaction between

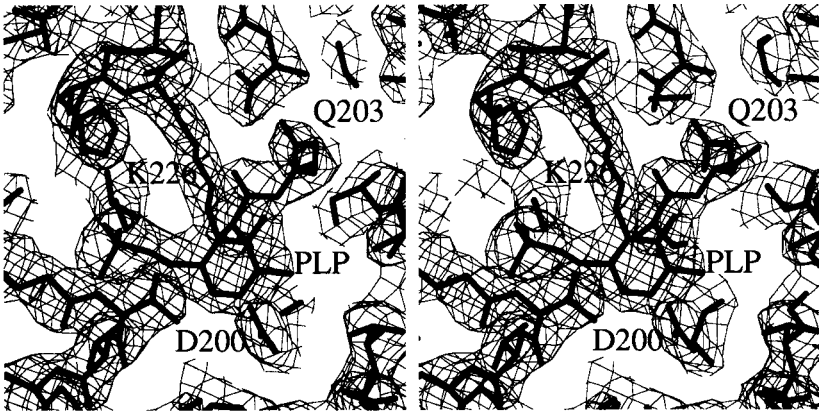

FIGURE 2: Stereoview of the $2F_o - F_c$ map contoured at the 1.5σ level, showing interactions between PLP and its neighboring residues. The figure was depicted with the program BOBSCRIPT (*47*).

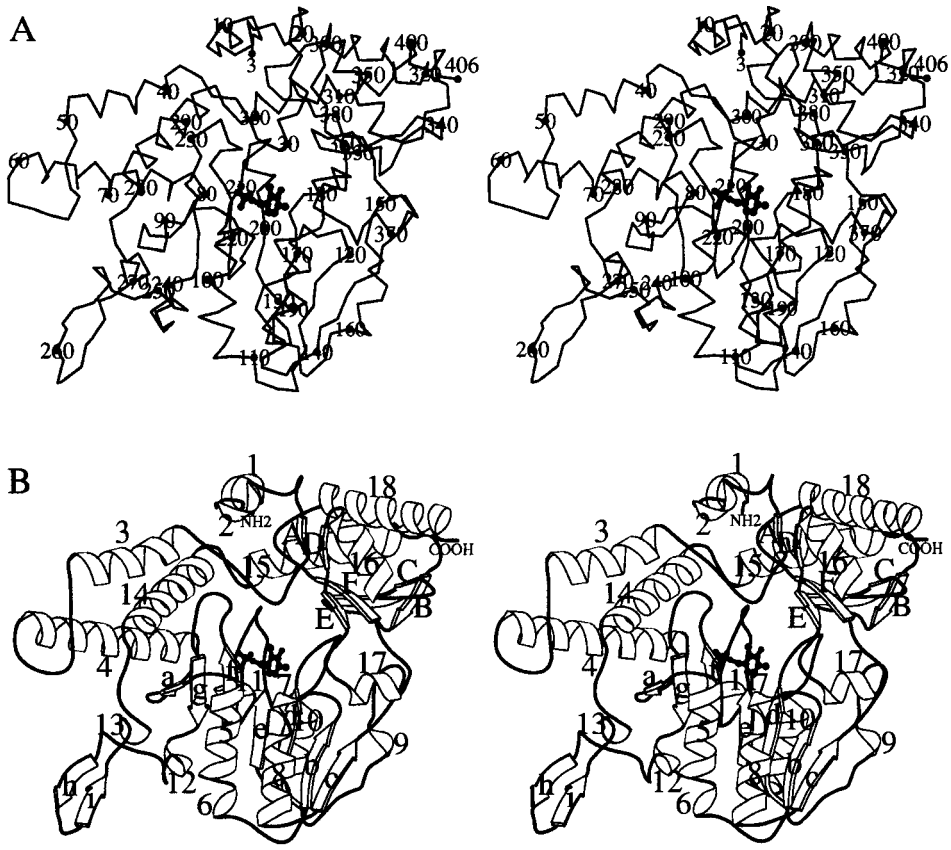

FIGURE 3: Stereoviews of the α-carbon trace (A) and the schematic drawing (B) of the CsdB subunit. The current model comprises 404 residues (Phe3−Gly406) with omission of two N-terminal disordered residues. In panel B, α- and 3_{10}-helices are represented by spirals and β-strands by arrows. Both figures were drawn with the program MOLSCRIPT (*48*).

the subunits in the dimer is large; the solvent accessible surface area of about 3200 Å^2 per subunit is buried upon dimer formation, corresponding to 19.9% of the whole accessible surface area of the subunit. The molecular 2-fold axis runs across the middle of helices 3 and 3* through the area surrounded by the N-termini of helices 14 and 14* and PLP-binding helices 5 and 5* and the C-termini of helices 8 and 8*. Consequently, intimate association between two subunits in the dimer is established by intersubunit interactions in the active site through several hydrogen bonds and hydrophobic interactions. In the intersubunit interface, α-helix 17 in the lobe extending from the small domain of one subunit interacts with the β-hairpin loop protruding from the large domain of the other subunit. These two portions, the extended lobe of one subunit and the protruded β-hairpin loop from the other subunit, form one side of a limb of the active site in the enzyme. Each of the active sites is formed by residues coming out from both subunits of the dimer. These intersubunit interactions which are involved in active site formation in the dimeric molecule are remarkable structural features in CsdB.

Structural Comparison with Other PLP-Dependent Enzymes. PLP-dependent enzymes are grouped into seven fold types, and fold-type I, including NifS homologues, is further divided into several subtypes based on the homology of their amino acid sequences (*19*). NifS homologues, including CsdB, are classified as the "aminotransferases class V of fold-type I" family of PLP-dependent enzymes. Enzymes

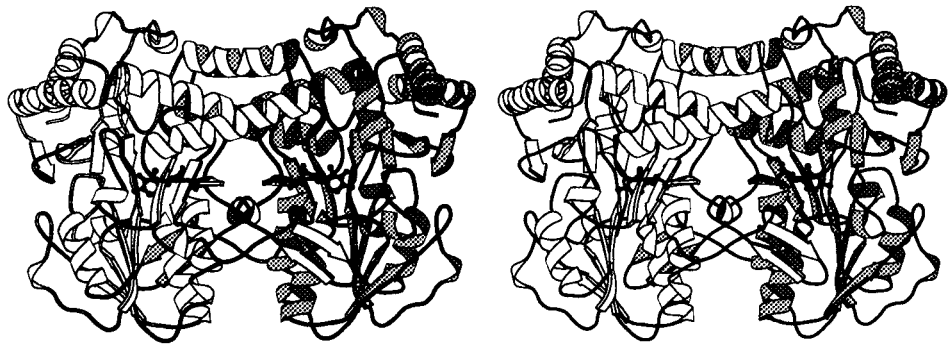

FIGURE 4: Stereoviews of the dimeric molecule of CsdB viewed perpendicularly to the molecular 2-fold axis. The figure, showing a pair of subunits shaded differently, was drawn with the program MOLSCRIPT (*48*).

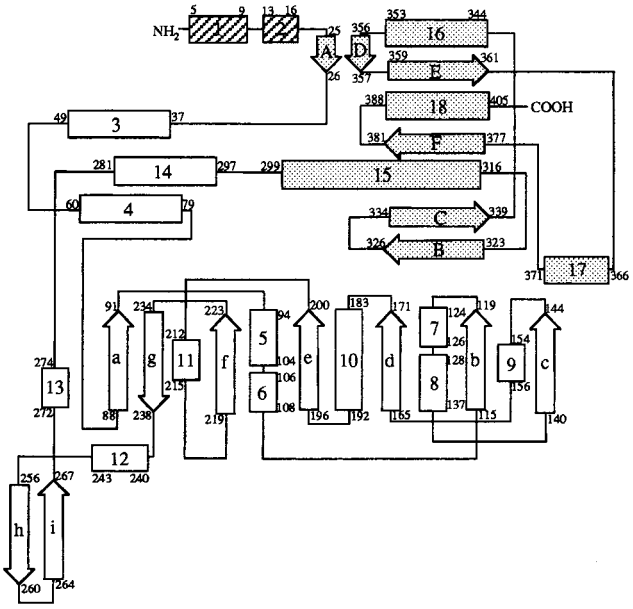

FIGURE 5: Topology diagram of the secondary structural elements of CsdB. α- and 3_{10}-helices are represented by rectangles and β-strands by arrows. The first and last residue numbers for each element are shown. The large PLP-binding domain, the small domain, and the N-terminal segment are shown as white boxes, gray boxes, and boxes with oblique lines, respectively.

belonging to the fold-type I family have two structural features as an identifiable signature within their sequences. First, the Schiff base lysine (Lys226 in CsdB) is closer to the C-terminus than the glycine-rich region (residues 93−97 in CsdB) and directly follows a hydrophobic β-strand. Second, an invariant aspartic acid residue (Asp200 in CsdB) which binds the nitrogen atom of the pyridine ring precedes the Schiff base lysine by 20−50 amino acid residues.

The aminotransferases class V of fold-type I includes NifS homologues, PSAT, serine-pyruvate aminotransferase, isopenicillin N epimerase, and the small subunit of cyanobacterial soluble hydrogenase. A search for structural homologues of CsdB with the program DALI (*33*) identified three-dimensional structures of seven proteins belonging to the fold-type I family: PSAT (*22*), 2,2-dialkylglycine decarboxylase (*34*), tryptophanase (*35*), cystathionine β-lyase (CBL) (*36*), aspartate aminotransferase (AAT) (*37*−*40*), glutamate semialdehyde aminotransferase (*41*), and bacterial ornithine decarboxylase (*42*), in order of score. Indeed, the Cα trace of the subunit of CsdB is well superposed on those of PSAT (Figure 6), a single class V enzyme with a known structure, and AAT (not shown), the most extensively studied fold-type I enzyme. The tertiary structure comparison of CsdB with the seven structures identified above clearly shows that several helices flanking the central β-sheet of the large domain in the class V enzymes of PSAT and CsdB are shorter than those of the other classes of enzymes. In CsdB, two regular α-helices of the large domain in other PLP-dependent enzymes of the fold-type I family are replaced with one-turn α- and 3_{10}-helices (11 and 9), as observed in the structure of PSAT (*22*). Moreover, the small domains in both class V enzymes are compact in comparison with those of the other classes of enzymes in the fold-type I family. These structural features are probably common to the class V family in fold-type I of PLP-dependent enzymes. All of the secondary structural elements except those of helices 1−3 in CsdB are well superposed on the corresponding ones of PSAT.

The most remarkable structural feature in CsdB lies in the interaction between the lobe containing α-helix 17 in one subunit of the dimer and the β-hairpin loop connecting strands h and i in the other subunit. The lobe exists between β-strands E and F, extending from the small domain to the large domain in the same subunit. α-Helix 17 on the lobe in one subunit of the dimer interacts with the tip of the β-hairpin loop from the other subunit through hydrophobic interactions, including that between Pro367 of the former subunit and Val259* of the latter. The lobe and the β-hairpin loop in CsdB are found neither in the other classes of PLP-dependent enzymes of the fold-type I family nor in PSAT, which belongs to the class V family. In PSAT, the β-hairpin loop in CsdB is replaced with an α-helix (residues 228−233). A short loop of PSAT that protrudes between β-strands E and F does not contain an α-helix and is shorter than the protrusion of CsdB by 13 residues. Thus, the interaction between the lobe and the β-hairpin loop observed in CsdB is not found in the other PLP-dependent enzymes.

Active Site Structure. The CsdB dimer has two active sites which exist separately in two equivalent clefts formed at the interface of two subunits in the dimer. The PLP molecule is settled at the bottom of the active site cleft, and the substrate must approach the PLP site through the cleft. Figure 7 shows the active sites of CsdB, AAT, and PSAT. The circumstances of active site in these enzymes are similar. As is found in the fold-type I family of PLP-dependent enzymes, PLP has the C4′ atom connected with the Nζ atom of Lys226, providing the Schiff base for forming an internal aldimine. The O3′ atom of PLP is hydrogen-bonded with the Nζ atom of Lys226 and with the Nε2 atom of Gln203. The pyridine

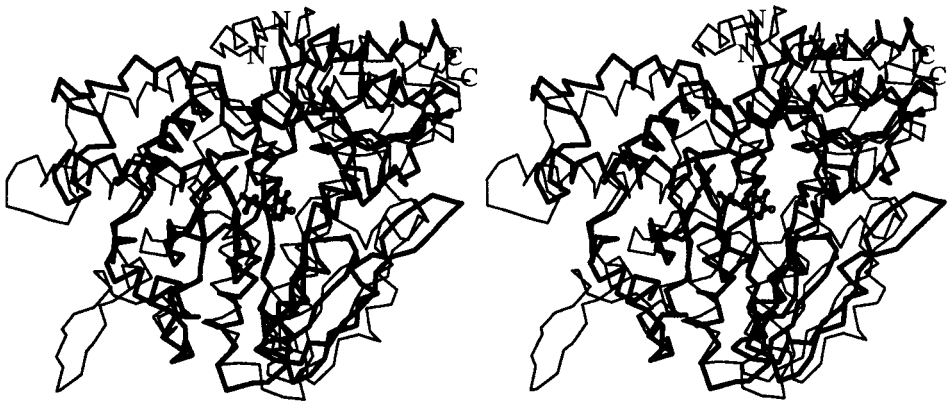

FIGURE 6: Stereoview of the superposition of CsdB (thin line) and PSAT (thick line; PDB code 1BJN). The superposition was carried out with the program DALI (*33*). The figure was generated using the program MOLSCRIPT (*48*).

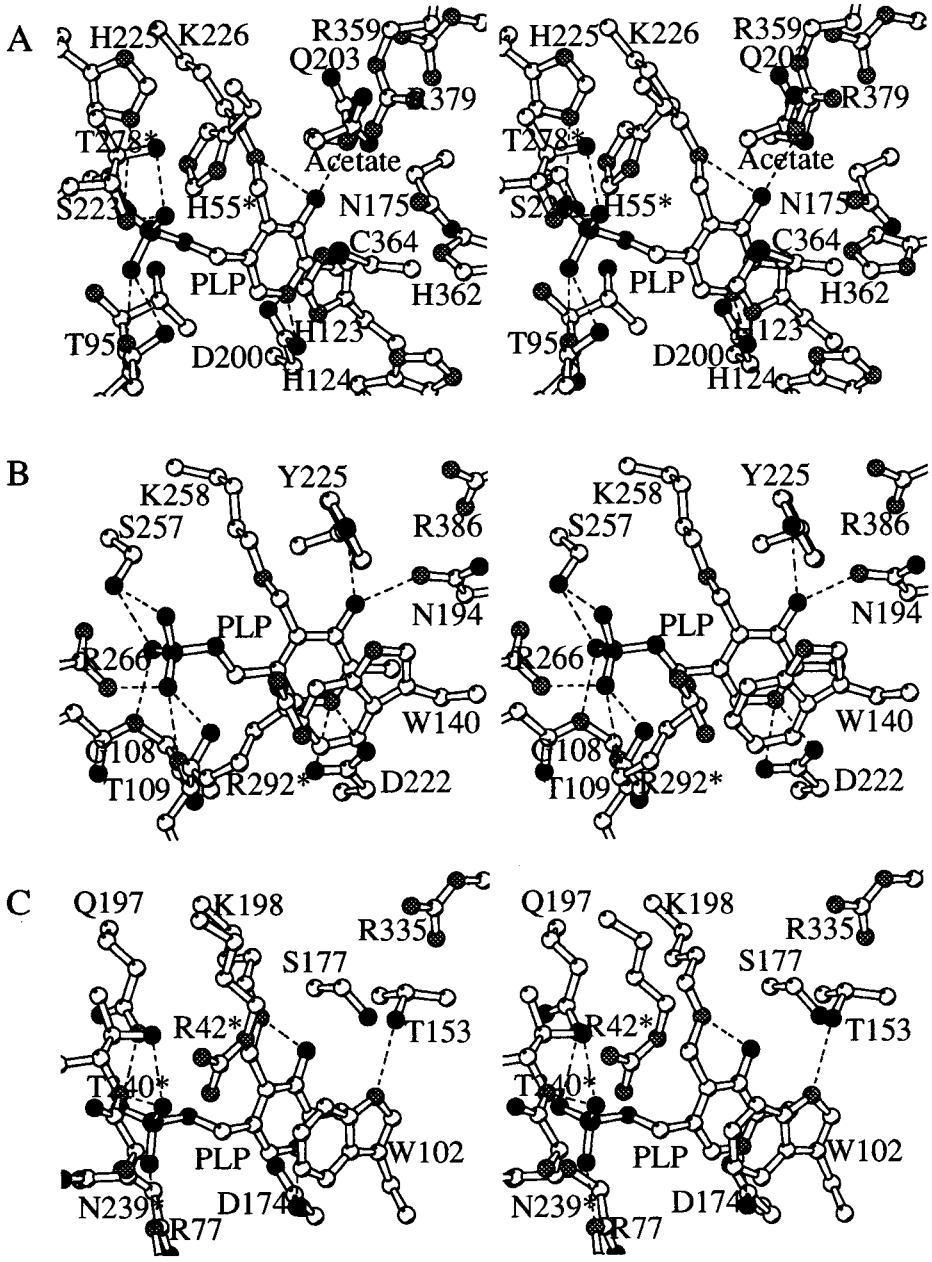

FIGURE 7: Active sites of CsdB (A), AAT (B), and PSAT (C). The hydrogen-bond network is shown in broken lines. Water molecules in the active sites are not shown for clarity. The figures were generated using the program MOLSCRIPT (*48*).

nitrogen atom N1 of PLP forms a hydrogen bond with Asp200. Asp200 in CsdB, which corresponds to Asp222 in AAT, probably stabilizes the protonated N1 of PLP to strengthen the electron-withdrawing capacity of the coen-

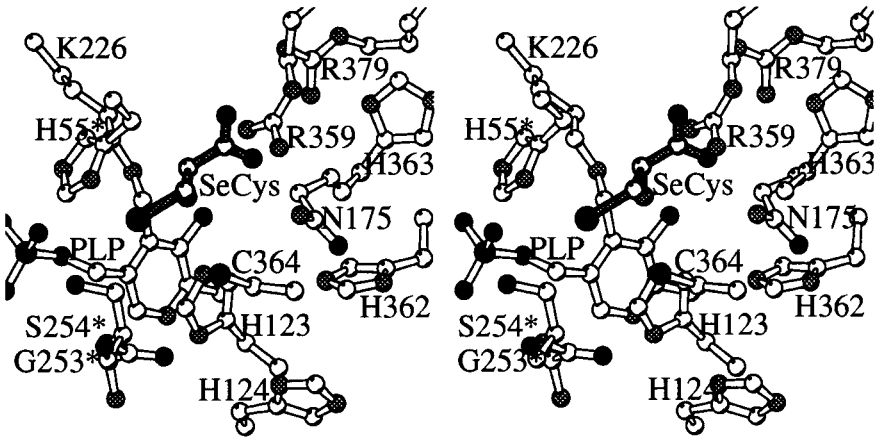

FIGURE 8: Ball-and-stick representation of the active site of CsdB, showing the expected binding mode of a substrate. The shaded L-selenocysteine molecule is modeled into the active site as the substrate. The figure was generated with the program MOLSCRIPT (*48*).

zyme (*43*). Thus, Asp200, Gln203, and Lys226 interact with PLP in a manner similar to that observed in AAT, which is supposed to affect the electron distribution on PLP. The OP2 atom of PLP is hydrogen-bonded with the side chain Oγ and main chain N atoms of Thr95 from one subunit of the dimer; the OP3 atom is hydrogen-bonded with the side chain Oγ atom of Ser223 and the side chain Nϵ2 atom of His225 from the same subunit, and the OP1 atom makes a hydrogen bond with the side chain Oγ and main chain N atoms of Thr278* from the other subunit.

The residue recognizing the carboxylate group at Cα of the substrate is Arg386 in AAT. Arg379 in CsdB is spatially well superposed on Arg386 in AAT and hydrogen-bonded with the carboxyl oxygen of the acetate ion found in the crystal presented here. The side chain of Asn175 is also hydrogen-bonded with the carboxyl group of the acetate ion. Thus, Arg379 and Asn175 in CsdB probably serve as the recognition residues for the α-carboxyl group of the substrate.

Although AAT, PSAT, and CsdB are similar to one another in most of the interactions between protein residues and PLP as well as the overall folding of protein, there are some differences among these enzymes; one of them lies in the stacking mode of the aromatic residue and the pyridine ring of PLP. In CsdB, the imidazole ring of His123 is stacked against the *re* face of the pyridine ring in PLP, while the stacking residues are Trp in AAT and PSAT. There are other cases in which aromatic residues such as Tyr and Phe are used for this stacking in cystathionine β-lyase from *E. coli* (*36*) and tyrosine phenol-lyase from *Citrobacter freundii* (*44*), respectively. Stacking of the histidine residue in this manner has also been reported in the crystal structures of ornithine decarboxylase from *Lactobacillus* 30a (*42*) and serine hydroxymethyltransferase from human cytosol (*45*).

Possible Modification of Cys364. A noticeable structural feature in the active site of CsdB is a possible modification of the side chain of Cys364, which is located near the pyridine ring of PLP. This cysteine residue corresponds to Cys325 in NifS of *A. vinelandii*, which is necessary for the activity of the enzyme (*8*) (Figure 1). Interestingly, the size of the electron density cloud for the side chain of Cys364 in CsdB is relatively larger than those of the other cysteine residues in the CsdB molecule. The size of the corresponding peak in the electron density map suggests the modification of the Cys364 side chain by a single atom. Because the structure has been analyzed at a medium resolution of 2.8 Å, it is difficult to determine the kind of atom for this modification. However, a report on the persulfide formation of the catalytic cysteine residue in NifS (*8*) suggests the possibility that Cys364 of CsdB was modified to −SSH or −SSeH after the catalytic reaction, although the size of the density peak at the modification site is smaller than those expected for ordered persulfide or selenosulfide with full occupancy. Cys364 may be modified to the −SSH or −SSeH form with high mobility and/or low occupancy.

The side chain of Cys364 is encompassed with the side chains of His123 and His124. The nitrogen atoms in the imidazole rings of these histidines positioned on the distal side of Cys364 make hydrogen bonds with the main chain amides, the hydrogen bond of His123 Nδ1 with Ala125 N being 3.0 Å long and that of His124 Nϵ2 with Met366 N being 2.9 Å long. This geometry indicates that these nitrogen atoms of the histidine residues are deprotonated. Consequently, the hydrogen-bound nitrogen atoms, Nϵ2 of His123 and Nδ1 of His124, face the Sγ atom of Cys364 at distances of 3.8 and 4.6 Å, respectively. The side chain of His362 is also directed toward Cys364 (4.9 Å). Cys364 is surrounded by these three histidine residues on three sides. The other side of Cys364 is occupied by Arg359, and the Sγ atom of Cys364 is close to the Nη1 and Nη2 atoms of Arg359 (4.8 Å).

DISCUSSION

Putative Binding Mode of the Substrate. The initial stage of the reaction of CsdB probably proceeds in a manner similar to those of other PLP enzymes in the fold-type I family such as AAT, since interactions and distributions of residues around PLP are similar to those of these PLP enzymes. Figure 8 shows the expected mode of binding of a substrate selenocysteine to the active site of CsdB based on the crystal structures of complexes of AAT with the substrate analogue, maleate or 2-methyl-L-aspartate (*38*, *39*), and PSAT with 2-methyl-L-glutamate (*22*). Selenocysteine is so modeled that its α-carboxyl group is roughly superposed on that of the acetate ion found in the crystal structure of CsdB presented here, and that the substrate interacts with PLP which is rotated by approximately 20° toward the outside of the active site, as is observed in the complexes of both enzymes. Thus, the location of the selenocysteine in

Scheme 1

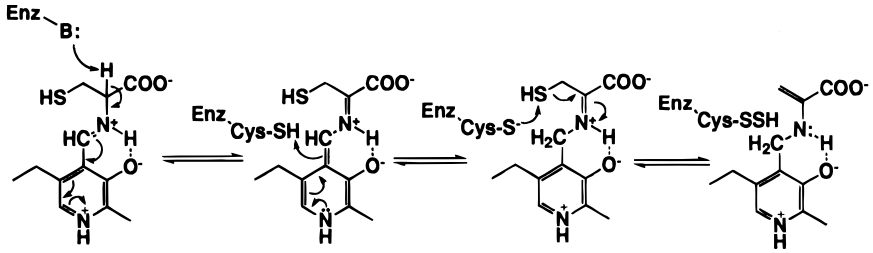

Scheme 2

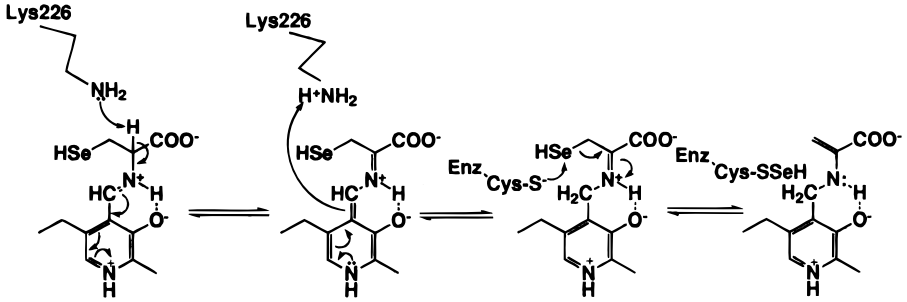

the present model of the selenocysteine−enzyme complex presumably represents that of the substrate moiety of the substrate−PLP adduct in the external aldimine intermediate.

In the model of the CsdB complex, the α-carboxyl group of the substrate is recognized with Arg379 and Asn175. The α-amino group of the substrate is oriented to the C4′ atom of PLP. Subsequently, the amino acid substrate would make the external aldimine with PLP by forming the Schiff base between the amino group of the substrate and the C4′ atom of PLP. His55* projecting from the other subunit in the dimer is the putative recognition residue for the side chain of the substrate in CsdB because this residue is located on the extension of the side chain of the modeled substrate and corresponds to Arg42* of PSAT, which is the recognition residue for the γ-carboxyl group of the complexed α-methyl-L-glutamate (*22*). In AAT, the side chain carboxylate of a substrate aspartate is recognized by the side chain of Arg292* from the other subunit of the dimer. In CsdB, however, the position corresponding to that of Arg292* in AAT is in the vicinity of Ser254*, too distant to interact with the side chain of the substrate.

Implications for the Catalytic Mechanism. In the modeled complex, the selenium at the γ-position of the substrate is close to the side chains of several residues such as Cys364 (about 5 Å) and His55* (about 4 Å). These residues are candidates for the catalytic residues of CsdB. A reaction mechanism involving a cysteine residue was proposed for the NifS enzyme (*8*). In the proposed mechanism, the proton is transferred from the −SH group of the Cys residue to the C4′ atom of PLP after the formation of the external aldimine (Scheme 1); subsequently, the cysteinyl thiolate anion generated in the active site makes a nucleophilic attack on the sulfur of the cysteine−PLP adduct, and finally, the cysteinyl persulfide and the enamine derivative of the alanine are formed. The alignment in amino acid sequence between the CsdB presented here and *A. vinelandii* NifS suggests that Cys364 could be a catalytic residue in CsdB (Figure 1).

As described above, Cys364 exists on the extending lobe from the small domain. The sulfur atom of Cys364 is located close to the γ-position of the modeled substrate, indicating that they can interact with each other (Figure 8). This result is consistent with the mechanism proposed by Zheng et al. for the NifS enzyme (*8*). However, the distance from the Sγ atom of Cys364 to the C4′ atom of PLP is too long for direct interaction (7.5 Å). Therefore, the proton transfer from the −SH group of Cys364 to the C4′ of PLP may not occur in CsdB. In the catalytic reaction of CsdB, Lys226 probably deprotonates the α-proton of the substrate and protonates the C4′ atom of PLP, as proposed for other PLP-dependent enzymes such as Lys258 in AAT (*37*), Lys198 in PSAT (*22*), and Lys210 in CBL (*36*) (Scheme 2).

The −SH group of Cys364 must be deprotonated to perform a nucleophilic attack on the γ-position of the substrate. It might appear that His123 and His124, which are located in the vicinity of Cys364, contribute to the deprotonation. However, this is probably not the case because hydrogen-bound nitrogen atoms of these residues face the Sγ atom of Cys364, as described above (see the Results). For the present, we speculate that His362 may play a role in the deprotonation of Cys364. His362 is slightly too distant (4.9 Å) for a direct hydrogen bond from the Sγ atom of Cys364. However, there seems to be no other putative candidate for this purpose in the vicinity of Cys364. His55*, corresponding to residue His37* which has been proposed on the basis of the PSAT structure to deprotonate the catalytic cysteine residue Cys325 in NifS (*22*), is probably not a suitable candidate for deprotonation because the distance (6.1 Å) between the Sγ atom of Cys364 and His55* is longer than that between the Sγ atom and His362.

An alternative mechanism that does not involve a nucleophilic attack by Cys364 is also possible (Scheme 3). This mechanism as well as that shown in Scheme 2 involves a 1,3-prototropic shift, as reported in AAT by Julin and Kirsch (*46*). According to the mechanism depicted in Scheme 3, the selenohydryl group of the selenocysteine−PLP adduct is deprotonated, and subsequently, the elemental selenium is released from the adduct. His55* is the catalytic base most probably extracting the proton from the selenium atom of

Scheme 3

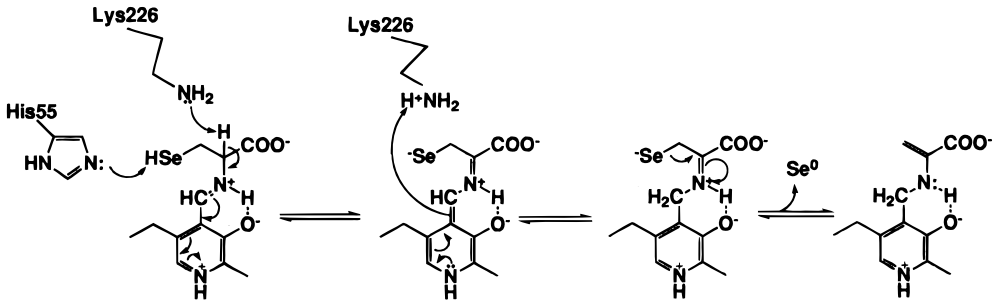

the substrate. However, the deprotonation of the selenohydryl group may occur without the aid of His55* because the pK_a value of the selenohydryl group is low (about 5.2).

The examination of the role of Cys364 by site-directed mutagenesis showed that selenocysteine degradation is not affected by the replacement of Cys364 with Ala and that the residue is required only for cysteine desulfurization (H. Mihara, T. Kurihara, T. Yoshimura, and N. Esaki, unpublished results). Accordingly, the CsdB reaction probably proceeds through the Scheme 2 mechanism for L-cysteine and through the Scheme 3 mechanism for L-selenocysteine.

Structural Comparison with Other NifS Homologues. As mentioned above, three NifS homologues of CsdB, CSD, and IscS exist in *E. coli*. The ratios of specific activity for L-selenocysteine to that for L-cysteine, the so-called discrimination factors, are 290, 6.9, and 8.2 for CsdB, CSD, and IscS, respectively (*18*). Thus, CsdB has high specific activity against L-selenocysteine compared with L-cysteine, while CSD and IscS display much higher activity against L-cysteine than CsdB.

NifS homologues are classified into two groups, namely groups I and II, on the basis of their degrees of sequence similarity (*10*). NifS from *A. vinelandii* and IscS are included in group I and CSD and CsdB in group II. CsdB closely resembles CSD in terms of amino acid sequence (44% identical). The important residues in CsdB for interacting with PLP and participating in the catalytic reaction are completely conserved in CSD (Figure 1). The marked differences between the sequences of CsdB and CSD lie in the regions of residues 40−90, 130−160, and 300−340 of CsdB, which are expected to have different conformations between the two enzymes. His55 of CsdB and His51 of CSD, which are located in the region of residues 40−90, may cause differences in the catalytic reaction between CsdB and CSD.

The CsdB structure in Figure 9 shows the regions (A−D) with markedly different sequences between group I (NifS and IscS) and group II (CSD and CsdB) NifS homologues. It should be noted that most of the regions (regions A, C, and D in Figures 1 and 9) are distributed in or around the active site. It is plausible that differences in functional properties among these enzymes are attributed to structural differences in these sequence-different regions. The amino acid sequence of the loop region containing His55 in CsdB (region A) is not homologous with those of NifS and IscS. This histidine in CsdB, which is conserved in group II NifS homologues, might play a role in catalysis or recognition of the substrate side chain. Group I NifS homologues also have a conserved histidine residue in region A (His41 in IscS and His37 in NifS), although the position of the residue is slightly different from that in the group II enzymes. The sequence dissimilarity in this loop region may affect the position of the histidine residue and result in differences in functional properties among NifS homologues.

The β-hairpin loop of residues 256−268 (region C), which contains strands h and i and makes up one side of the active site in CsdB, is deleted in IscS and NifS. In contrast to this deletion, 10 residues are inserted in IscS and NifS between the residues corresponding to Met366 and Pro367 on α-helix 17 of CsdB (residues 366−371) (region D). The region just follows the putative catalytic residue Cys364. Therefore, the extended lobe anchoring the catalytic cysteine residue seems to be much larger in IscS and NifS than in CsdB and to have a different structure as well as a different location of the catalytic cysteine residue between the former two enzymes and the latter. The low activity of CsdB against L-cysteine may be caused by the longer distance between the γ-atom of the substrate and the possible catalytic residue Cys364, relative to that in IscS which exhibits a higher activity than CsdB.

The lobe extending from the small to the large domains of the subunit and containing the putative catalytic cysteine residue is the most remarkable structural feature common to the NifS homologues and probably a prerequisite for the proteins to function as SCL and cysteine desulfurase. This structure is not found in other "fold-type I" PLP-dependent

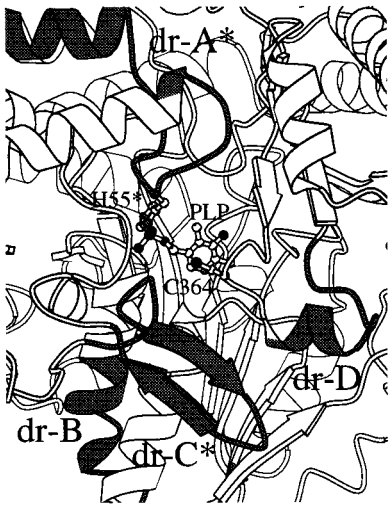

FIGURE 9: Schematic representation of CsdB showing structural differences between CsdB and NifS. Their structurally different regions, which are denoted in Figure 1, are shaded and labeled "dr-B" for residues 99−115 and "dr-D" for residues 366−376 from one subunit and "dr-A*" for residues 34−60 and "dr-C*" for residues 251−268 from the other subunit. PLP, Cys364, and His55* are depicted as ball-and-stick models. Helices and β-strands are represented by spirals and arrows, respectively. The figure was drawn with the program BOBSCRIPT (*47*).

enzymes. Moreover, His55 from the other subunit is positioned so that it interacts with the γ- or β-atom of the substrate and may be involved in the catalytic reaction. Structural analyses of other NifS homologues, including IscS and CSD, will clarify the relationship between the molecular structure and the catalytic properties of NifS homologues.

REFERENCES

1. Esaki, N., Nakamura, T., Tanaka, H., and Soda, K. (1982) *J. Biol. Chem. 257*, 4386−4391.
2. Chocat, P., Esaki, N., Tanizawa, K., Nakamura, K., Tanaka, H., and Soda, K. (1985) *J. Bacteriol. 163*, 669−676.
3. Lacourciere, G. M., and Stadtman, T. C. (1998) *J. Biol. Chem. 273*, 30921−30926.
4. Veres, Z., Kim, I. Y., Scholz, T. D., and Stadtman, T. C. (1994) *J. Biol. Chem. 269*, 10597−10603.
5. Forchhammer, K., and Böck, A. (1991) *J. Biol. Chem. 266*, 6324−6328.
6. Neuhierl, B., and Böck, A. (1996) *Eur. J. Biochem. 239*, 235−238.
7. Stadtman, T. C. (1996) *Annu. Rev. Biochem. 65*, 83−100.
8. Zheng, L., White, R. H., Cash, V., and Dean, D. R. (1994) *Biochemistry 33*, 4714−4720.
9. Zheng, L., White, R. H., Cash, V. L., Jack, R. F., and Dean, D. R. (1993) *Proc. Natl. Acad. Sci. U.S.A. 90*, 2754−2758.
10. Mihara, H., Kurihara, T., Yoshimura, T., Soda, K., and Esaki, N. (1997) *J. Biol. Chem. 272*, 22417−22424.
11. Flint, D. H. (1996) *J. Biol. Chem. 271*, 16068−16074.
12. Sun, D., and Setlow, P. (1993) *J. Bacteriol. 175*, 1423−1432.
13. Kolman, C., and Söll, D. (1993) *J. Bacteriol. 175*, 1433−1442.
14. Wilson, R., Ainscough, R., Anderson, K., Baynes, C., Berks, M., Bonfield, J., Burton, J., Connell, M., Copsey, T., Cooper, J., Coulson, A., Craxton, M., Dear, S., Du, Z., Durbin, R., Favello, A., Fraser, A., Fulton, L., Gardner, A., Green, P., Hawkins, T., Hiller, L., Jier, M., Johnston, L., Jones, M., Kershaw, J., Kirsten, J., Laisster, N., Latreille, P., Lightning, J., Lloyd, C., Mortimore, B., O'Callaghan, M., Parsons, J., Percy, C., Rifken, L., Roopra, A., Saunders, D., Shownkeen, R., Sims, M., Smaldon, N., Smith, A., Smith, M., Sonnhammer, E., Staden, R., Sulston, J., Thierry-Mieg, J., Thomas, K., Vaudin, M., Vaughan, K., Waterston, R., Watson, A., Weinstock, L., Wilkinson-Sproat, J., and Wohldman, P. (1994) *Nature 368*, 32−38.
15. Nakai, Y., Yoshihara, Y., Hayashi, H., and Kagamiyama, H. (1998) *FEBS Lett. 433*, 143−148.
16. Land, T., and Rouault, T. A. (1998) *Mol. Cell 2*, 807−815.
17. Zheng, L., Cash, V. L., Flint, D. H., and Dean, D. R. (1998) *J. Biol. Chem. 273*, 13264−13272.
18. Mihara, H., Maeda, M., Fujii, T., Kurihara, T., Hata, Y., and Esaki, N. (1999) *J. Biol. Chem. 274*, 14768−14772.
19. Grishin, N. V., Phillips, M. A., and Goldsmith, E. J. (1995) *Protein Sci. 4*, 1291−1304.
20. Rozzell, J. D. (1991) U.S. Patent 5019509.
21. Koushik, S. V., Sundararaju, B., McGraw, R. A., and Phillips, R. S. (1997) *Arch. Biochem. Biophys. 344*, 301−308.
22. Hester, G., Stark, W., Moser, M., Kallen, J., Markovic-Housley, Z., and Jansonius, N. (1999) *J. Mol. Biol. 286*, 829−850.
23. Matthews, B. W. (1968) *J. Mol. Biol. 33*, 491−498.
24. Collaborative Computational Project, Number 4 (1994) *Acta Crystallogr. D50*, 760−763.
25. Furey, W., and Swaminathan, S. (1990) *American Crystallographic Association Meeting Abstracts 18*, 73.
26. Abrahams, J. P., and Leslie, A. G. W. (1996) *Acta Crystallogr. D52*, 30−42.
27. Kleywegt, G. J., and Jones, T. A. (1996) *Acta Crystallogr. D52*, 826−828.
28. Jones, T. A., Zou, J.-Y., and Cowan, S. W. (1991) *Acta Crystallogr. A47*, 110−119.
29. Brünger, A. T. (1992) *X-PLOR, Version 3.1: A system for Crystallography and NMR*, Yale University Press, New Haven, CT.
30. Cambillau, C. (1992) *Turbo-FRODO, version 5.02*, BioGraphics, Marseille, France.
31. Brünger, A. T. (1992) *Nature 355*, 472−474.
32. Laskowski, R. A. (1993) *J. Appl. Crystallogr. 26*, 283−291.
33. Holm, L., and Sander, C. (1993) *J. Mol. Biol. 233*, 123−138.
34. Toney, M. D., Hohenester, E., Cowan, S. W., and Jansonius, J. N. (1993) *Science 261*, 756−759.
35. Isupov, M. N., Antson, A. A., Dodson, E. J., Dodson, G. G., Demetieva, I. S., Zakomirdina, L. N., Wilson, K. S., Dauter, Z., Lebedev, A. A., and Harutyunyan, E. H. (1998) *J. Mol. Biol. 276*, 603−623.
36. Clausen, T., Huber, R., Laber, B., Pohlenz, H.-P., and Messerschmidt, A. (1996) *J. Mol. Biol. 262*, 202−224.
37. Kirsch, J. F., Eichele, G., Ford, G. C., Vincent, M. G., Jansonius, J. N., Gehring, H., and Christen, P. (1984) *J. Mol. Biol. 174*, 497−525.
38. Jäger, J., Moser, M., Sauder, U., and Jansonius, J. N. (1994) *J. Mol. Biol. 239*, 285−305.
39. Okamoto, A., Higuchi, T., Hirotsu, K., Kuramitsu, S., and Kagamiyama, H. (1994) *J. Biochem. 116*, 95−107.
40. Ree, S., Silva, M. M., Craig Hyde, C., Rogers, P. H., Metzler, C. M., Metzler, D. E., and Arnone, A. (1997) *J. Biol. Chem. 272*, 17293−17302.
41. Hennig, M., Grimm, B., Contestabile, R., John, R. A., and Jansonius, J. N. (1997) *Proc. Natl. Acad. Sci. U.S.A. 94*, 4866−4871.
42. Momany, C., Ernst, S., Ghosh, R., Chang, N.-L., and Hackert, M. L. (1995) *J. Mol. Biol. 252*, 643−655.
43. Yano, T., Kuramitsu, S., Tanase, S., Morino, Y., and Kagamiyama, H. (1992) *Biochemistry 31*, 5878−5887.
44. Antson, A. A., Demidkina, T. V., Gollnick, P., Dauter, Z., Von Tersch, R. L., Long, J., Berezhnoy, S. N., Phillips, R. S., Harutyunyan, E. H., and Wilson, K. S. (1993) *Biochemistry 32*, 4195−4206.
45. Renwick, S. B., Snell, K., and Baumann, U. (1998) *Structure 6*, 1105−1116.
46. Julin, D. A., and Kirsch, J. F. (1989) *Biochemistry 28*, 3825−3833.
47. Esnouf, R. M. (1997) *J. Mol. Graphics Modell. 15*, 132−134.
48. Kraulis, P. J. (1991) *J. Appl. Crystallogr. 24*, 946−950.

BI991732A